Which Features Trigger Action Potentials in Cortical Neurons *in Vivo*?

Holger Fröhlich
Center for Bioinformatics Tübingen (ZBIT)
Sand1, 72076 Tübingen, Germany
Email: froehlic@informatik.uni-tuebingen.de

Björn Naundorf
Dept. Nonlinear Dynamics
Max-Planck Institute for Dynamics and Self Organization
Göttingen, Germany
Email: bjoern@chaos.gwdg.de

Maxim Volgushev
Dept. Neurophysiology MA 4/149
Ruhr-Universität Bochum, Germany
Email: maxim@neurop.ruhr-uni-bochum.de

Fred Wolf
Dept. Nonlinear Dynamics
Max-Planck Institute for Dynamics and Self Organization
Göttingen, Germany
Email: fred@chaos.gwdg.de

***Abstract*— We study the initiation of action potentials (APs) in *in vivo* recordings of cortical neurons from cat visual cortex. Recently, it was shown that cortical neurons are not simple threshold devices, emitting an AP each time a fixed voltage threshold is reached, but that the emission of an AP partly depends on the rate of change of the membrane potential preceeding an AP. In this paper we investigate systematically which features of the membrane potential lead to an AP by means of Machine Learning methods. We use Support Vector Machines (SVMs) to discriminate between trajectories of the membrane potential which lead to an AP within the next τ ms and trajectories which do not lead to the initiation of an AP. For every point in a trajectory of the membrane potential (MP) we compute a set of 11 features and use a forward selection algorithm to find out the relevant features for the occurence of an AP. Based on the results we construct a reduced prediction model. This model suggests that AP occurences can be predicted best by a combination of the 1st temporal derivative of the MP at distance τ to the AP maximum, the MP itself and the mean MP over a longer range.**

I. Introduction

The human brain is the most complex information processing device known to date. Its basic computational units are neural cells which dynamically transform synaptic inputs into action potentials (APs) by an intrinsically nonlinear process. This process enables networks of neurons to perform complex computations [10], [11], [7]. Classically, neurons are viewed as integrators, summing synaptic inputs and emitting an AP once the neurons' membrane potential (MP) reaches a threshold voltage. This reductionistic view was extended by Hodgkin and Huxley [6] who developed a biophysical theory, which could explain the generation of APs. They showed that the emission of an AP is a non-linear high-dimensional process involving the detailed dynamics of voltage-dependent channels in the membrane of a neuron. Although major advances were achieved in describing the dynamics of the underlying voltage-gated channels individually in great detail, emergent mechanisms which result from their dynamical interplay were investigated only recently [8], [1]. In these studies it was predicted that the voltage at which an AP initiates partially depends on the velocity with which the membrane potential depolarates. This prediction was confirmed in recent experiments, which investigated the generation of APs in cortical neurons. They demonstrated that APs initiate at a low voltage when the membrane potential depolarized quickly and at a high voltage when the membrane potential depolarizes slowly [2].

From a functional point of view the mechanism of AP initiation has a strong qualitative impact on the information processing in the brain. In simplified models it was demonstrated that seemingly minor details of the AP generating mechanism can fundamentally alter the nature of the encoding of synaptic inputs into sequences of APs, as shown in [5], [12].

The goal of this paper is to clarify, which features of the MP lead to the occurence of an AP in cortical neurons *in-vivo*. For this purpose we investigated 9 *in-vivo* recordings of neurons from cat visual cortex. Neurons *in-vivo* are subject to an immense synaptic bombardment, leading to large fluctuations of their MP. Although the functional role of these fluctuations is still unclear, it significantly alters the neurons' dynamical properties [4], [16]. We analyzed the AP generation in this "natural environment" and examined which patterns in the subthreshold fluctuations of the MP could predict best the occurrence of an AP. To do this, we defined a set of 11 features, which we computed for every MP point in a recording.

To discriminate MP trajectories leading to APs from those which did not lead to the generation of an AP, we employed Support Vector Machines (SVMs). SVMs belong to the family of "Kernel Methods" [13], [15], [14] and are one of the most popular Machine Learning methods today. Without making any a-priori assumptions about the relevance of certain features, we used a forward selection algorithm [9] to find out the features which contributed most to the classification in each dataset. From all feature subsets that were selected for a single recording we infered a reduced model, which

incorporated only those three features that were top ranked for all traces. These were the 1st temporal derivative and the height of the MP at AP onset, as well as the mean AP 5ms prior AP onset. We evaluated the reduced model on all datasets and showed that indeed the classification performance was at least as good as when using all 11 features. Our results thus suggest that the occurence of an AP is mostly determined by the mean potential over a longer range, the height of the potential shortly before the AP and the 1st temporal derivative of the membrane potential shortly before the AP. Thereby the feature with the largest impact was the first temporal derivative whereas the influence of the two other features was significantly lower. In conclusion our results imply that the AP generation mechanism in cortical neurons *in vivo* acts rather as a coincidence detector than as an integrator.

In the next section we will first give a brief review on SVMs and highlight the relevant features for our study. Afterwards we will describe our method in detail. In section III we present the results of the application of our method on *in-vivo* recordings from cat visual cortex. In section IV we summarize our results and conclude.

II. Methods

A. Support Vector Machines - a Brief Review

Support Vector Machines (SVMs) were introduced in 1995 by V. Vapnik and C. Cortes [3], [15], [14] and are one of the most popular Machine Learning methods today: Given some empirical dataset $\mathcal{D} = \{(x_i, y_i) \in \mathcal{X} \times \{\pm 1\} | i = 1, ..., N\}$ with $x_i \in \mathcal{X}$ being observations in some arbitrary input domain and $y_i \in \{\pm 1\}$ the class labels we want to construct a decision hyperplane $f(x) = \text{sign}\left(\langle \mathbf{w}, \phi(x) \rangle + b\right)$ in some Hilbert space $\mathcal{H}$. Thereby $\phi : \mathcal{X} \to \mathcal{H}$ is a (possibly nonlinear) map of the original data into *feature space* $\mathcal{H}$. The hyperplane is constructed such that *margin size* (that is the distance of the hyperplane to points closest to it in feature space) is maximal. This is achieved by solving the quadratic program

$$\begin{aligned} &\min_{\mathbf{w},\xi,b} \frac{1}{2}\|\mathbf{w}\|^2 + \frac{C}{N}\sum_{i=1}^{N}\xi_i \\ &\text{subject to } y_i(\langle \mathbf{w}, \phi(x_i)\rangle + b) \geq 1 - \xi_i \\ &\xi_i \geq 0 \end{aligned} \tag{1}$$

where $C > 0$ is a constant that regularizes the trade-off between minimizing the training error $\frac{1}{N}\sum \xi_i$ and maximizing the size of the margin $1/\|\mathbf{w}\|$ in feature space. Equivalently one can solve the dual of (1):

$$\begin{aligned} &\max_{\alpha} \sum_i \alpha_i - \frac{1}{2}\sum_{i,j}\alpha_i\alpha_j y_i y_j \langle \phi(x_i), \phi(x_j)\rangle \\ &\text{subject to } \sum_i \alpha_i y_i = 0 \\ &\alpha_i \in (0, C] \end{aligned} \tag{2}$$

Thereby the apearing dot products $\langle \phi(x_i), \phi(x_j)\rangle$ in (2) can be implicitly computed via a so called *kernel function* $k : \mathcal{X} \times \mathcal{X} \to \mathbb{R}$. Popular examples of kernel functions are e.g. the radial basis function, which allows nonlinear class separation, but also the ordinary dot product $\langle \cdot, \cdot \rangle$ can be viewed as a special kernel (the linear kernel) with the property $\mathcal{X} = \mathcal{H}$ and $\phi = id$.

A special property of SVMs is, that only points for which $\alpha_i \neq 0$ contribute to the decision function. They are called *support vectors* (SVs). Geometrically they correspond to points lying on or within the margin. They are the extreme examples within each class, i.e. examples which are most similar to those of the opposite class. In fact by removing all training examples except the support vectors one recovers the same solution as when using all data. This property is called *sparseness* of the solution.

An alternative formulation to the so called C-SVM Eq. (1), introduced by Schölkopf [13] is the ν-SVM:

$$\begin{aligned} &\min_{\mathbf{w},\xi,\rho,b} \frac{1}{2}\|\mathbf{w}\|^2 - \nu\rho + \frac{1}{N}\sum_{i=1}^{N}\xi_i \\ &\text{subject to } y_i(\langle \mathbf{w}, \phi(x_i)\rangle + b) \geq \rho - \xi_i \\ &\xi_i \geq 0, \rho \geq 0 \end{aligned} \tag{3}$$

Here $\rho/\|\mathbf{w}\|$ is the size of the margin in feature space and $\nu \in (0, 1]$ the regularization constant. Schölkopf et al. proved that ν is both, an upper bound on the fraction of training errors and a lower bound on the fraction of support vectors. Furthermore, for $N \to \infty$ ν equals both, the fraction of training errors and the fraction of support vectors [13]. Like for the C-SVM a dual formulation for (3) can be found which allows the usage of arbitrary kernel functions.

We now turn to the description of our method, which employs SVMs as an essential tool for classification, in detail.

B. Our Approach

1) In-vivo *Recordings:* We analyzed 9 *in-vivo* recordings from cat visual cortex, where each recording contained at least 100 APs. The recordings exhibited only spontaneous activity, generated from the surrounding network, leading to low firing rates < 2Hz. The experimental details and the data acquisition are published in [17]. Each recording consists of a discrete time trajectory $T_V = \{(t_i, V(t_i)) | i = 1, ..., N\}$ of length N with membrane potentials $V(t_i)$ at times points t_i. All datesets except the last 3 were recorded at a time resolution of 0.1ms while the last three had a resolution of 0.05ms. The times of the AP maxima in the following are denoted by $\hat{t}_1, ..., \hat{t}_\ell$.

2) Preprocessing and Feature Construction: We first low-pass filtered all recordings using a 5-point sliding window average. The MP at every point t_i was embedded in a 11-dimensional feature space, resulting in a vector $\mathbf{x}(t_i)$. The single coordinates of the feature space were defined as:

- the MP $V(t_i)$
- the 1st to 5th derivatives $\frac{d^k V}{dt^k}(t_i)$ of the MP
- the mean MP potentials $\overline{V}_r(t_i), r = 0.5, 1, 2.5, 10$ms before t_i.

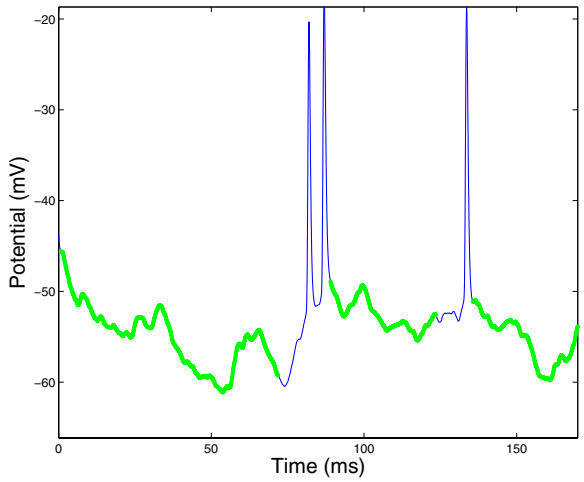

Fig. 1. Small piece of an example trajectory with negative examples marked thicker.

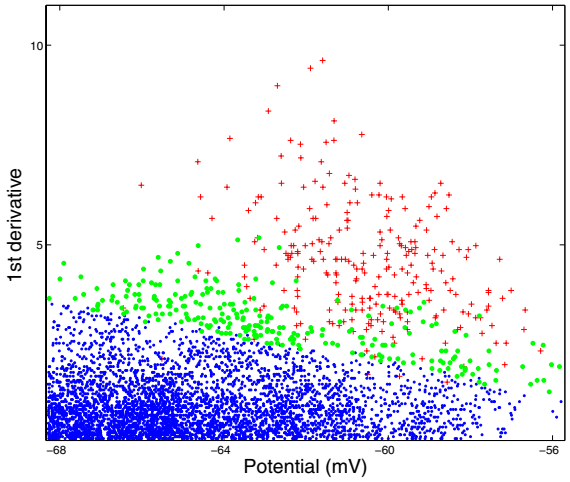

Fig. 2. Example of the first two features of positive ('+') and negative examples (dots) plotted against each other ($\tau = 0.7$ms). The subsampled negative support vectors are marked thicker. Positive and negative examples overlap with regard to all features individually (see text).

3) Negative Examples: We next constructed the set of those examples $\{\mathbf{x}_i^{(n)}\}$, which do not lead to the generation of an AP. They will be called *negative examples* in the following. They were chosen such that their distance was more than 10ms to the following AP and more than 2ms from the preceeding AP (Fig. 1). This safety distance excluded the small trajectories between two burst APs and ensured that negative examples were not close to the AP initiation where active conductances play an important role.

4) Positive Examples: As the set of *positive examples* $\{\mathbf{x}_i^{(p)}\}$ we chose all trajectories ending at time points $\tilde{t}_j - \tau$. Thereby the time points $\tilde{t}_j$ are all those times of AP maxima $\hat{t}_j$ which have a time distance of at least 10ms to the preceeding AP. This procedure reliably removed all burst APs.

Obviously, for small distances τ, the set of positive and negative examples can be trivially distinguished by the height of the MP. To ensure that the classification is not trivial we increased the value of τ in steps of 0.1ms until the two sets could not be separated by a threshold with regard to any feature. The distance was then further increased until the number of points which overlapped in any feature was at least as large as the number of APs in the whole recording. Figure 2 illustrates this construction by showing the first feature plotted against the second feature. Both classes overlap and a simple threshold separation in the first or second feature individually is not possible. The positions $\tilde{t}_j - \tau$ are in the following also called the onset positions of APs.

5) Subsampling of Negative Examples : Compared to the length of the whole trajectory T_V, a AP is a quite rare event. This implies that in a recording we have only few positive examples compared to a huge number of negative examples (approx. 10^5 as many as positive examples). To achieve a high accuracy of our classifier and to reduce the computational cost we thus selected a subset of negative examples, which were most similar to the set positive examples, i.e. which

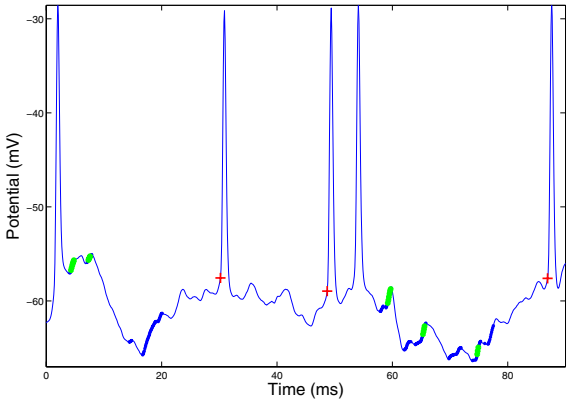

Fig. 3. Positive and negative examples in an example trajectory ($\tau = 0.7$ms). End points of positive examples are marked with red crosses, end points of negative examples are marked a little bit thicker than the rest of the trajectory. Selected support vectors are marked with big green dots. Negative examples are all those which overlap with the positive ones with regard to all features plus or minus one standard deviation (see text). Note that the third AP is neglected, because it follows the previous AP too closely.

were hardest to classify. Obvious candidates for this are those negative examples which overlap with the positive ones. To have a sufficient coverage of the whole space we extended this set of overlapping negatives by all those negatives which lay within one standard deviation of the features of the positive examples.

Figure 2 shows a scatter plot, graphing the first two features of positive and negative examples. The number of negative examples m' (dots) exceeds the number of positive examples m (crosses) by several orders of magnitude. Training a SVM with this data would lead to an unnecessary computational burden. On the other hand, a uniform random subsampling of

the negative examples would produce many examples which are quite far away from our decision line and hence do not contribute to the classification, i.e. they are not support vectors. This would lead to a suboptimal performance of the classifier. Thus our goal should be to select our negative training data among those which will likely become support vectors later. As we know from subsection II-A, for ν-SVMs the parameter ν is a lower bound on the fraction of support vectors. Hence, by setting $\nu = 2m/(m' + m)$ and training a SVM on the whole data, we get approximately $2m$ support vectors of which around m should be negative examples. This firstly leads to a nicely balanced dataset and secondly it automatically produces those examples, we should concentrate on during training. Note that we are not interested in the decision hyperplane itself here, but just in the selected support vectors. In Fig. 2 the selected negative examples are marked by thick green dots. The SVM training was performed using a linear kernel, and the data was normalized to mean 0 and standard deviation 1 before training. To get a better impression, Fig. 3 displays an example trajectory with overlapping negative examples and selected support vectors. Alltogether we now have a set of positive examples (crosses) and a set of negative examples (big dots) which can be used to design a model. Only these two sets were considered in the following in order to find out the relevant features.

6) Finding Out The Relevant Features in a Recording: To find out the relevant features in a recording we employed a forward selection algorithm [9]. Starting with an empty set of features, we successively added those feature which, if added to the existing ones, lead to the lowest 5-fold cross-validation error. This procedure was continued until all features had been included. The order of inclusion into the feature set induces a ranking of the features. In the end the feature set with the lowest cross-validation error was returned.

During the feature selection we used a linear $C-$SVM, because in general training is a little bit faster compared to the ν-SVM. We chose the parameter C via a 5-fold cross-validation from the grid $2^{-4}, ..., 2^5$ at each stage of the feature selection algorithm. Like above, before training each feature for the whole data was normalized to mean 0 and standard deviation 1.

7) Construction of a Generalized Reduced Model: As a result of the forward selection algorithm we obtained a ranked feature subset for each recording which could classify best the positive and negative examples in the training set. It is, however, not a-priori clear that a feature set, which performs well on one recording will also perform as good on another recording, i.e. if the prediction model generalizes well across different recordings. We thus constructed a reduced model in which we included only those features, which were ranked most frequently among the 5 best features for each single recording.

8) Evaluation of the Reduced Model: This reduced model was evaluated subsequently for every recording using 5-fold cross-validation. Thereby each training set consisted of 4/5 of the examples obtained by the procedure described in II-B.5 and the testing set of *all* examples in the recording that were not used for training. As before, a linear C-SVM was used. To prevent overfitting the parameter C was adapted via an extra level of 5-fold cross-validation within each cross-validation procedure. To determine the relative impact of each feature on the classification, we computed the weight vector $\mathbf{w}$ of the decision hyperplane:

$$\mathbf{w} = \sum_i \alpha_i y_i \mathbf{x}_i$$

were α_i are the Lagrangian multipliers obtained by solving the quadratic program Eq. (2). This was possible, because we used a linear kernel. The absolute value $|w_j|$ can be viewed as a measure for the relative influence (weight) of feature j on the decision hyperplane $f(\mathbf{x}) = \text{sign}\left(\langle \mathbf{w}, \mathbf{x} \rangle + b\right)$. During the evaluation we computed the mean of the weight vectors over all cross-validation folds for each recording, and normalized each compound of the mean weight vector by its standard deviation.

TABLE I

OVERVIEW OF THE DIFFERENT DATASETS USED IN OUR EXPERIMENTS.

Dataset	#AP	#Test Instances	#Negative SVs	τ(ms)
1	121	216661	121	1.1
2	188	1376364	188	0.6
3	177	38241	178	0.9
4	258	22400	259	0.7
5	252	27028	253	0.7
6	183	41674	183	0.7
7	128	1463434	128	0.6
8	1098	2909598	1097	0.6
9	385	3867932	385	0.6

III. RESULTS

We applied our method to 9 *in-vivo* recordings of spontaneous activity from cat visual cortex. Table I shows an overview of the different datasets with respect to the number of APs, the selected distance τ from AP maxima, the number of subsampled negative examples (negative SVs) selected by the ν-SVM and the number of overall test examples.

Table II shows which features were selected for each dataset in the order of their inclusion together with the 5-fold cross-validation error on the reduced set of examples obtained by the procedure described in section II-B.5.

We then evaluated how frequent each feature was ranked among the first 5 (table III). Including only those features which were ranked among the first 5 in at least 50% of all cases we constructed a reduced model, which incorporated the following features:

- the mean potential over a longer range (i.e. $\bar{V}_5$)
- the membrane potential at AP onset (i.e. at $\tilde{t}_i - \tau$)
- the 1st derivative of the membrane potential at AP onset

We tested the generalized model on all recordings as described in the previous section. The number of false negatives (FN) and the number of false positives (FP) are listed together with the relative false negative (fnr) and false positive rates (fpr) in table IV. The relative false negative rate is defined

TABLE II

SELECTED FEATURES FOR 9 REAL LIFE DATASETS IN THE ORDER THEY WERE INCLUDED AND 5-FOLD CROSS-VALIDATION ERROR (%) ± STANDARD DEVIATION (%).

Recording	Features	CV error (%)
1	$\frac{dV}{dt}$, V, $\bar{V}_5$, $\bar{V}_1$, $\bar{V}_{0.5}$	5.33 ± 3.12
2	$\frac{d^2V}{dt^2}$, V, $\frac{dV}{dt}$, $\frac{d^4V}{dt^4}$, $\bar{V}_{0.5}$, $\bar{V}_{2.5}$, $\bar{V}_{10}$, $\frac{d^3V}{dt^3}$, $\frac{d^5V}{dt^5}$, $\bar{V}_1$	0.79 ± 0.72
3	$\frac{dV}{dt}$, $\bar{V}_1$, $\bar{V}_{10}$, $\frac{d^2V}{dt^2}$, $\frac{d^4V}{dt^4}$, $\bar{V}_5$, $\bar{V}_{2.5}$, $\frac{d^5V}{dt^5}$, V	15.07 ± 2.39
4	$\frac{dV}{dt}$, $\bar{V}_{0.5}$, $\bar{V}_5$, $\frac{d^5V}{dt^5}$, V	4.25 ± 2.86
5	$\frac{dV}{dt}$, V, $\bar{V}_{10}$, $\frac{d^2V}{dt^2}$, $\bar{V}_{0.5}$, $\bar{V}_{2.5}$, $\bar{V}_{0.5}$, $\frac{d^4V}{dt^4}$, $\frac{d^3V}{dt^3}$, $\frac{d^5V}{dt^5}$, $\bar{V}_1$	3.96 ± 1.86
6	$\frac{dV}{dt}$, $\bar{V}_1$, $\bar{V}_5$, $\frac{d^3V}{dt^3}$, $\frac{d^4V}{dt^4}$, $\frac{d^5V}{dt^5}$, $\bar{V}_{10}$, $\bar{V}_{0.5}$, $\bar{V}_{2.5}$, V, $\frac{d^2V}{dt^2}$,	7.89 ± 5.75
7	$\frac{dV}{dt}$, V, $\bar{V}_5$, $\frac{d^2V}{dt^2}$, $\frac{d^3V}{dt^3}$, $\frac{d^5V}{dt^5}$, $\bar{V}_{2.5}$, $\bar{V}_1$, $\bar{V}_{0.5}$, $\bar{V}_{10}$, $\frac{d^4V}{dt^4}$	5.05 ± 1.74
8	$\frac{dV}{dt}$, V, $\bar{V}_{10}$, $\frac{d^2V}{dt^2}$, $\frac{d^5V}{dt^5}$, $\bar{V}_5$, $\frac{d^4V}{dt^4}$, $\bar{V}_{0.5}$, $\frac{d^3V}{dt^3}$, $\bar{V}_1$	5.33 ± 1.12
9	$\frac{dV}{dt}$, V, $\bar{V}_{2.5}$, $\frac{d^3V}{dt^3}$, $\bar{V}_{10}$, $\frac{d^4V}{dt^4}$, $\frac{d^2V}{dt^2}$, $\bar{V}_1$, $\frac{d^5V}{dt^5}$, $\bar{V}_5$	9.22 ± 2.26

TABLE III

ANALYSIS OF THE FREQUENCY OF THE RANKING OF THE FEATURES AMONG THE FIRST BEST ONES IN ALL DATASETS.

Feature	#Selected	%	Among First 5	%
V	9	100	**7**	**77**
V_{10}	7	77	4	44
V_5	7	77	**5**	**55**
$V_{2.5}$	6	66	1	11
V_1	8	89	3	33
$V_{0.5}$	7	77	3	33
$\frac{dV}{dt}$	9	100	**9**	**100**
$\frac{d^2V}{dt^2}$	7	77	4	44
$\frac{d^3V}{dt^3}$	6	66	3	33
$\frac{d^4V}{dt^4}$	7	77	2	22
$\frac{d^5V}{dt^5}$	8	89	1	11

as $fnr = FN/NEG$, and the relative false positive rate as $fpr = FP/POS$ with POS being the number of positive examples and NEG the number of negative examples in the test set. Additionally, we tested against the usage of all features. The results of this experiment are shown in table V. Compared to the usage of all features, our reduced model in 7 cases leads to a significant improvement and to a significant detoriation in only 2 cases. The significance was tested separately for the number of false negatives and false positives by means of a paired t-test at significance level 5%. This shows that in general the reduced model, which incorporated only features that we assumed to be most relevant for the occurence of an AP, has a better generalization capability than the full model using all features. This nicely corroborates our generalized model.

We finally investigated the relative influence of each of the three most relevant features on the decision hyperplane by means of the mean weight vector obtained on each recording. Figure 4 shows a histogram of the mean weight vector components divided by the 1-norm of the vector and averaged over all recordings. The influence of the mean potential over the last 5ms is comparable to the potential at AP onset, while the 1st derivative on average has a much higher impact. This result is consistent with the ranking obtained in table II.

TABLE IV

RESULTS ON THE EVALUATION EXPERIMENT USING OUR REDUCED MODEL: NUMBER OF FALSE NEGATIVES (FN), OF FALSE POSITIVES (FP), AND RELATIVE FALSE NEGATIVE (FNR) AND FALSE POSITIVE RATE (FPR) ± STANDARD DEVIATION. SIGNIFICANT IMPROVEMENTS IN COMPARISON TO THE USAGE OF ALL FEATURES ARE MARKED BY "*", DETORIATIONS BY "-".

dataset	FN	FP	fnr (%)	fpr (%)
1	2.2 ± 1.3	$63 \pm 8.2^-$	9.13 ± 5.47	0.02 ± 0.01
2	0.8 ± 0.8	0.8 ± 1.3	2.12 ± 2.21	0 ± 0
3	$3.2 \pm 1.5^*$	$2 \pm 1.2^*$	9 ± 4.16	0.01 ± 0
4	3.6 ± 1.3	1.6 ± 1.1	6.97 ± 2.56	0.01 ± 0.01
5	$4 \pm 1.4^-$	$2.2 \pm 1.5^*$	7.95 ± 2.82	0.01 ± 0.01
6	$0.2 \pm 0.4^*$	$0.4 \pm 0.5^*$	0.54 ± 1.21	0 ± 0
7	2.6 ± 3.1	1.6 ± 1.1	10.25 ± 12.57	0 ± 0
8	25.6 ± 6.5	$10 \pm 1.6^*$	11.65 ± 2.97	0 ± 0
9	11 ± 2.2	$52 \pm 4.2^*$	14.29 ± 2.9	0.01 ± 0

TABLE V

RESULTS ON THE EVALUATION EXPERIMENT USING ALL FEATURES: NUMBER OF FALSE NEGATIVES (FN), OF FALSE POSITIVES (FP), AND RELATIVE FALSE NEGATIVE (FNR) AND FALSE POSITIVE (FPR) RATE ± STANDARD DEVIATION.

dataset	FN	FP	fnr (%)	fpr (%)
1	2.6 ± 1.1	26 ± 8.3	10.8 ± 4.81	0.01 ± 0.01
2	0.6 ± 1.3	0.4 ± 0.5	1.57 ± 3.53	0 ± 0
3	6 ± 1.2	27.8 ± 15.3	16.8 ± 3.33	0.07 ± 0.04
4	3 ± 1.2	3.2 ± 2.1	5.81 ± 2.34	0.01 ± 0.01
5	1.8 ± 0.8	10.4 ± 2.9	3.58 ± 1.69	0.04 ± 0.01
6	4 ± 2.6	9.6 ± 3.85	10.89 ± 6.87	0.02 ± 0.01
7	2.2 ± 2.3	1 ± 1	8.65 ± 9.16	0 ± 0
8	13.8 ± 4	142.2 ± 71.5	6.28 ± 1.8	0.01 ± 0
9	8.6 ± 1.8	87.6 ± 7.5	11.17 ± 2.36	0.02 ± 0

IV. CONCLUSION

We investigated the AP generation in *in-vivo* recordings from cat visual cortex. We introduced an empirical method to work out which features of the trajectory of the membrane potential are most relevant for the occurence of an AP. Based on statistical tools, namely Support Vector Machines, we developed a technique to infer a model automatically from empirical data. Without making any a-priori assumptions about the relevance of certain features, we used a forward selection algorithm to find features which discriminated well between trajectories leading to an AP and others which do not. Based on the results for each of our recordings we constructed a reduced model, which only included the MP, the rate of change of the MP and the MP averaged over 5ms. Using this reduced model, APs could be predicted with a very high accuracy on all

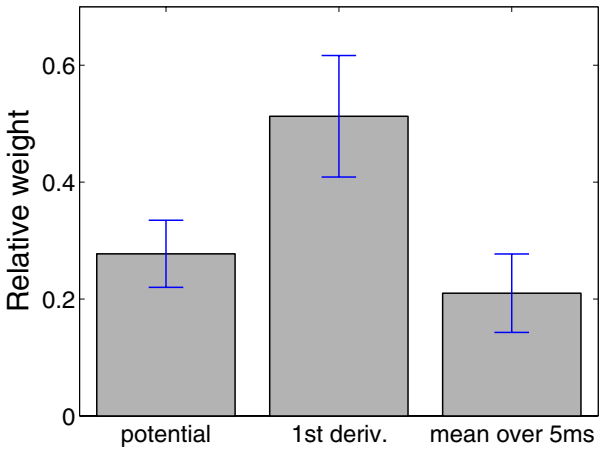

Fig. 4. Relative influence of the three most relevant features on the decision hyperplane averaged over all datasets.

our recordings, which reveals the high statistical consistency and generalization capability of our reduced model. Our results suggest that qualitatively the occurence of an AP is mostly determined by the mean potential over a longer range before AP, the height of the membrane potential shortly before the AP and the 1st temporal derivative of the membrane potential shortly before the AP. Surprisingly, the 1st temporal derivative of the MP had a much larger impact on the classification than the mean MP over a long range. This suggests that cortical neurons act as coincidence detectors, which are most sensitive to fast changes of the MP. Models of cortical neurons which assume a voltage threshold for AP initiation might not reflect the dynamics of AP generation of cortical neurons.

Several previous theoretical studies assessed the computation performed in single neurons (e.g. [8], [1]). These studies were almost exclusively based on the Hodgkin-Huxley model [6], which describes the dynamical interplay of voltage-gated sodium and potassium channels in the generation of an AP. It is, however, not a-priori clear that this dynamics is equivalent with the AP generation in cortical neurons. Experimentally, the AP generation in cortical neurons *in vivo* was recently addressed in [2] *in vivo*. In this study, a correlation between the potential and the first derivative at AP onset was proposed to explain the large variability of AP onset potentials found *in vivo*. Our approach generalizes these results by using a set of 11 features without any a-priori weighting. It therefore allowed for the systematic construction of a simple phenomenological models, which reproduces the AP generation with very high accuracy and serves as a starting point for the development for simplified phenomenological neuron models, which reproduce the dynamical AP initiation of cortical neurons *in vivo*.

REFERENCES

[1] B. Aguera y Arcas, A.L. Fairhall, W. Bialek. Computation in a single neuron: Hodgkin and Huxley revisited. *Neural Comp.*, 15, 1715-1749, 2003

[2] R. Azouz and C.M. Gray. Dynamic spike threshold reveals a mechanism for synaptic coincidence detection in cortical neurons in vivo. *PNAS*, 97, 8110-5, 2000.

[3] C. Cortes and V. Vapnik. Support vector networks. *Machine Learning*, 20:273–297, 1995.

[4] Destexhe A, Pare D. Impact of network activity on the integrative properties of neocortical pyramidal neurons in vivo. *J Neurophysiol.*, 81, 1531-47, 1999.

[5] Fourcaud-Trocmé N, Hansel D, van Vreeswijk C, Brunel N. How spike generation mechanisms determine the neuronal response to fluctuating inputs. *J Neurosci.*, 23, 11628-40, 2000.

[6] A.L. Hodgkin and A.F. Huxley. A quantitative description of ion currents and its applications to conduction and excitation in nerve membranes. *Journal of Physiology (London)*, 117:500–544, 1952.

[7] J.J. Hopfield. Neural networks and physical systems with emergent collective computational abilities. *PNAS*, 79, 2554–2558, 1982.

[8] C. Koch, O. Bernander, R.J. Douglas. Do neurons have a voltage or a current threshold for action potential initiation?, Comp. Neuroscience, 2, 63-82, 1995.

[9] R. Kohavi and G. John. Wrappers for Feature Subset Selection. *Artificial Intelligence*, 97(12):273 – 324, 1997.

[10] W. McCulloch and W. Pitts. A logical calculus of ideas immanent in nervous activity. *Bulletin of Mathematical Biophysics*, 5:115–133, 1943.

[11] M. Minsky and S. A. Papert. *Perceptron*. MIT Press, Cambridge, 1988.

[12] Naundorf B, Geisel T, Wolf F. (2004). Dynamical Response Properties of a Canonical Model for Type-I Membranes. *Neural Comp.*, In Press

[13] B. Schölkopf and A. J. Smola. *Learning with Kernels*. MIT Press, Cambridge, MA, 2002.

[14] V. Vapnik. *The Nature of Statistical Learning Theory*. Springer, New York, NY, 1995.

[15] V. Vapnik. *Statistical Learning Theory*. John Wiley and Sons, New York, 1998

[16] M. Volgushev, U.T. Eysel. Noise makes sense in neuronal computing. *Science*, 290, 1908-9, 2000.

[17] M. Volgushev, J. Pernberg, U.T. Eysel. Gamma-frequency fluctuations of the membrane potential and response selectivity in visual cortical neurons, *Eur. J. Neurosci.*, 17, 1768-1776, 2003.